# Identification of brain connectivity disruptions due to thalamic lesions in early development using Diffusion-Weighted MRI

Ana Rita Oliveira
a.rita.v.oliveira@tecnico.ulisboa.pt

Instituto Superior Técnico, Lisboa, Portugal

October 2018

**Abstract**

Continuous spike-wave of sleep (CSWS) is an age-related epileptic syndrome that affects mainly children. Although it has idiopathic etiology, an involvement of thalamic lesions has already been reported and accounts for 14% of the CSWS cases, representing the most common etiology. Leal et al. (2018) proposed a model for the genesis of CSWS in patients with unilateral thalamic lesions that consists of a partial thalamic-cortical disconnection, which expresses a frequency-dependent excitability at sleep spindle frequencies and therefore is able to create an augmenting response during the non-rapid eye movement (non-REM) sleep stages, potentially leading to CSWS. Diffusion-weighted imaging (DWI) is a technique sensitive to the microstructural organization of the tissues, that has been widely used to map the white matter pathways of the brain. It also enables to parcellate brain structures according to its connectivity profile, in a method known as connectivity-based parcellation. Four patients were selected from a population of children with CSWS associated with strictly unilateral thalamic lesions. The aim of this thesis was to use DWI to parcellate their thalamus into nuclei and therefore infer on the structural connectivity between each thalamic nucleus and the different regions in the cortex. Electroencephalogram (EEG) and functional magnetic resonance imaging (fMRI) data were also used to support the interpretations made. Results showed a posterior brain region more disconnected from the thalamus, in the hemisphere ipsilateral to the thalamic lesion, as well as more prone to paroxysmal activity. This supports Leal et al. (2018) hypothesis of a causal relationship between thalamocortical disconnectivity and the epileptic events.

**Keywords:** Diffusion-weighted MRI, tractography, CSWS, thalamic lesion, thalamus parcellation

## 1. Introduction

The thalamus is an important brain structure known to as a relay station or a hub and is composed of several nuclei, each relaying information to different cortical regions (Sherman and Guillery, 2013). During early neonatal development, these nuclei can be damaged, for instance due to thalamic hemorrhage and potentially lead to epileptic activity (Kersbergen et al., 2013). Continuous spike-wave of sleep (CSWS) is an age-related rare condition and important treatable epileptic encephalopathy and its connection to thalamic lesions has already been reported (Incorpora et al., 1999; Monteiro et al., 2001; Kelemen et al., 2006; Guzzetta et al., 2005). Thalamic lesions have been demonstrated to be the most common etiology, affecting 14% of a group of 100 children with CSWS, as demonstrated by Fernández et al. (2012b). The exact location of the thalamic lesion, or the nucleus affected, if mentioned in the study reports, is not always in agreement between cases. Nevertheless, recent studies suggest the involvement of the dorsomedial nucleus. Indeed, Losito et al. (2015) showed that thalamic lesions with predominately involvement of the mediodorsal nuclei lead to higher incidences of CSWS, in a ratio of 61% to 39%, when compared to other thalamic lesions.

CSWS is characterized, as described in Singhal and Sullivan (2014), by (1) seizures, (2) neurocognitive regression and (3) a specific EEG pattern called electrical status epilepticus in sleep (ESES). The latter, in its turn, is characterized by (1) the activation of epileptiform discharges during sleep, (2) the presence of continuous or near-continuous, bilateral or occasionally unilateral, slow-spikes-waves, and finally (3) the occurrence of these slow-spike-waves during a significant proportion (85%) of the non-rapid eye movement (non-REM) sleep. Discharges generally present a frequency between 1.5 to 3 Hz.

This syndrome, more than the other types of epilepsy, exhibits a very particular relationship with sleep. Actually, the classic hypothesis for the genesis of spike-waves during sleep (Fernández et al., 2012a) resides on a corruption of the physiological

mechanism of sleep spindles - a physiological oscillation of the brain occurring at around 10 to 15 Hz observed essentially in the non-REM sleep; the thalamus is a critical structure for its generation.

Sleep spindles are thought to provide a cortical stimulus with an appropriate frequency to potentiate a cortical augmenting response (Timofeev et al., 2002), which are progressively growing potentials elicited in the cerebral cortex with optimal frequency around 10 Hz (Steriade and Timofeev, 1997).

Leal et al. (2018) proposed a model for the genesis of CSWS in patients with unilateral thalamic lesions that consists of a partial thalamic-cortical disconnection expressing a frequency-dependent increased excitability at sleep spindle frequencies, which is able to create an augmenting response during the non-REM sleep stages, potentially leading to CSWS. Under this hypothesis, the identification of the several nuclei that compose the thalamus is necessary to infer on the structural connectivity between each thalamic nucleus and the several cortical regions.

To identify those nuclei, a conventional magnetic resonance image (MRI) is not adequate, since these images do not present sufficient contrast to enable distinguishing their boundaries. However, thalamic nuclei can be identified through a method known as connectivity-based parcellation (Cloutman et al., 2012). This approach parcellates brain structures into subregions, according to the distinct connections they make to the cortex, or, more generally, to other brain regions. For this purpose, it is necessary to map the white matter (WM) pathways running from that structure - in this case the thalamus - to the cortex. Diffusion-weighted magnetic resonance imaging (DWI) is a sensitive technique to diffusion of water molecules within the different biological compartments in the brain, therefore it is the MRI technique better suited for this WM mapping (Bastiani and Roebroeck, 2015).

The main objective of this thesis was to perform thalamic segmentation using DWI data collected in infants with CSWS associated with unilateral early thalamic lesions. This result was used to infer on the structural connectivity between each thalamic nucleus and the different cortical regions, supported by the hypothesis of a neocortical area partially deafferented from the thalamus, as suggested by Leal et al. (2018). To complement this analysis, results were also interpreted in conjunction with additional data acquired on the same patients, namely whole-night electroencephalography (EEG) recordings and simultaneous EEG-functional MRI (fMRI).

## 2. Implementation

### 2.1. Data acquisition

A group of four children were selected from a population of children with CSWS, evaluated by Dr. Alberto Leal at the Clinical Neurophysiology Laboratory of Hospital Júlio de Matos. All the patients presented a strictly unilateral thalamic lesion as assessed by the brain MRIs performed for clinical care.

For all patients a T1-weighted and a DWI were acquired. Imaging was performed on a 3T Siemens Verio scanner for subjects 1 and 2, and on a 1.5T GE Medical Systems Signa HDxt MR scanner for subjects 3 and 4.

For subjects 1 and 2, diffusion-weighted data were acquired using Echo Planar Imaging (EPI): TR/TE=7200/97 ms; fifty 2.3-mm-thick axial slices; matrix size, 96x96; field of view, 220.8 x 220.8 $mm^2$; giving a voxel size of 2.3 x 2.3 x 2.3 $mm^3$; with an isotropic distribution along 64 directions, using a b-value of 1000 $s/mm^2$. A volume with no diffusion-weighting was acquired at the beginning of the acquisition. The total scan time for the DWI protocol was $\sim$ 8 min. T1-weighted anatomical images were acquired with a gradient-echo MPRAGE sequence, using the following parameters: voxel size of 1 x 1 x 1 $mm^3$; in-plane matrix resolution 160 x 228, 220 slices and 160 x 240, 256 slices, for subjects 1 and 2, respectively; field of view 160 x 228 $mm^2$, 160 x 240 $mm^2$, for patients 1 and 2, respectively.

For subjects 3 and 4, diffusion-weighted data were acquired using an EPI sequence: TR/TE=9050/99.6 ms, forty 2.5-mm-thick axial slices for subject 3 and TR/TE=8450/105.5 ms, forty two 2.5-mm-thick axial slices for subject 4; matrix size, 256x256; field of view, 240.60 x 240.60 $mm^2$; giving a voxel size of 0.94 x 0.94 x 2.50 $mm^3$; with an isotropic distribution along 35 directions, using a b-value of 1000 $s/mm^2$. A volume with no diffusion-weighting was acquired at the beginning of the acquisition. The total scan time for the DWI protocol was $\sim$ 10 min. T1-weighted anatomical images were acquired with an ultrafast gradient-echo with magnetization preparation sequence (IR-FSPGR), using the following parameters: voxel size of 0.94 x 0.94 x 0.60 $mm^3$; in-plane matrix resolution 256 x 256; 292 and 284 slices, for subjects 3 and 4, respectively; field of view 240.60 x 240.60 $mm^2$.

For subject 2, a resting state functional MRI (rsfMRI) was also collected, in a 3 Tesla Siemens Verio scanner using a 2D multi-slice gradient-echo EPI sequence with the following parameters: TR/TE=2500/30 ms; in-plane matrix resolution 64 x 64; 40 slices (interleaved acquisition); voxel size = 3.5 x 3.5 x 3.0 $mm^3$. Session time consisted of 20 min. The EEG was recorded simul-

taneously using a 32-channel MR-compatible EEG system (BrainAmp MR plus amplifier, Brain Products, Germany). A BrainCap MR model (EasyCap, Herrsching, Germany) was used, with a standard montage according to the 10-20 system.

Whole-night EEG recordings were collected for all patients. The electrodes were placed directly on the subject's head following the 10-20 system. For patient 2 subtemporal electrodes (F9/10 and P9/10) were also used.

The main steps of the processing pipeline used in this work are depicted in Fig. 1. Analysis was performed using tools from the FMRIB Software Library (FSL) (`www.fmrib.ox.ac.uk/fsl`) and other softwares identified throughout the text.

### 2.2. Diffusion data analysis

*Preprocessing.* For each subject, DWI and T1-weighted images were skull-stripped with FSL's Brain Extraction Tool (BET) (Smith, 2002). T1-weighted scans were submitted to FMRIB's Automated Segmentation Tool (FAST) (Zhang et al., 2001) to derive partial volume estimates for grey matter (GM) and an anatomical scan corrected for the bias field. DWI data was corrected for geometrical distortions, using the *eddy* tool from FMRIB's Diffusion Toolbox (FDT) (Andersson and Sotiropoulos, 2016).

*Thalamic seed masks and cortical target regions.* In all patients, a mask of the whole thalamus was manually drawn in the T1-weighted image, following the methodology described in Power et al. (2015), with MRICron software (University of South Carolina). Cortical masks, to be used as targets in tractography, were defined using the Brainnetome atlas (Fan et al., 2016), according to known thalamic connection sites, as in Behrens et al. (2003a). Seven regions were delineated: Temporal, Prefrontal, Premotor cortex, Primary Motor Cortex, Somatosensory Cortex, Posterior Parietal and Occipital zones, illustrated in Fig. 2. Given that the masks obtained are in the MNI space, registration was applied to, firstly, transform them to the T1 space and, secondly, to the diffusion space (where tractography takes place). The first step was achieved through a linear followed by a non-linear registration with the Advanced Normalization Tools (ANTs) software (Avants et al., 2011). This algorithm appears to perform better when compared to some other softwares, such as FMRIB's Non-linear Image Registration Tool (FNIRT) (Klein et al., 2009). To include as targets only voxels with an estimated percentage of GM of more than 30%, this tissue, previously obtained with FAST, was thresholded at 30% and was then used to mask the resulted structural cortical regions. The second registration was carried out with a linear algorithm, using FMRIB's Linear Image Registration Tool (FLIRT) (Jenkinson and Smith, 2001). Thalamus masks were linear transformed into the diffusion space of each individual, using FLIRT.

*Tractography and connectivity-based classification* Initially, *bedpostx* (Behrens et al., 2007) was used to determine the diffusion parameters per voxel. This approach, also called, Balls & Sticks model, assumes a fully isotropic compartment - the ball - mixed with a perfectly anisotropic compartment - the stick. The orientation of the stick provides the preferred orientation of a fiber within a voxel. More than one stick can be considered by the model, which represents more than one fiber orientation per voxel. Only two fibres were modelled per voxel, given that in order to resolve more than 3 fibers per voxel, the algorithm would require b-values of more than 1000 s/mm$^2$. Also, since, some of the subjects DWI were acquired with 35 directions (less than the 60 recommended), a burn-in of 2000 was chosen, instead of the default 1000. This value refers to the number of iterations discarded before starting the sampling, which reduces the amount of saved data and ensures convergence of the Markov Chains used by the algorithm when the data is noisy, since it is unlikely that the initial simulations came from the intended distribution. This step was followed by *probtrackx* (Behrens et al., 2003b), where a total of 5000 samples were drawn to generate a connectivity distribution from voxels within the thalamus and each of the cortical masks previously defined. An additional mask of the middle sagittal plane was given, which prevented the pathways found to cross to the contralateral hemisphere. Hard segmentation was executed with *find_the_biggest* function (Behrens et al., 2003a), which classifies each thalamic voxel according to target mask which it had more connectivity to. The volume of each nucleus in each of the hemispheres was calculated in the diffusion space, to assess volume differences between hemispheres.

### 2.3. EEG data analysis

*Spike detection.* EEG data from all patients were submitted to a low-pass and notch filter of 70 Hz and 50 Hz, respectively, and underwent spike detection using the *Persyst* software (Scheuer et al., 2017).

*Spike clustering.* Spike clustering was also performed in the *Persyst* software. Spikes were grouped based on topology and morphology features - height, duration and tip angle - in an hierarchical fashion. The resulting dendrogram was opened until a leaf node (cluster) with degree of dissimilarity equal or inferior to 4 was found. These final clusters were visually inspected: bipolar clus-

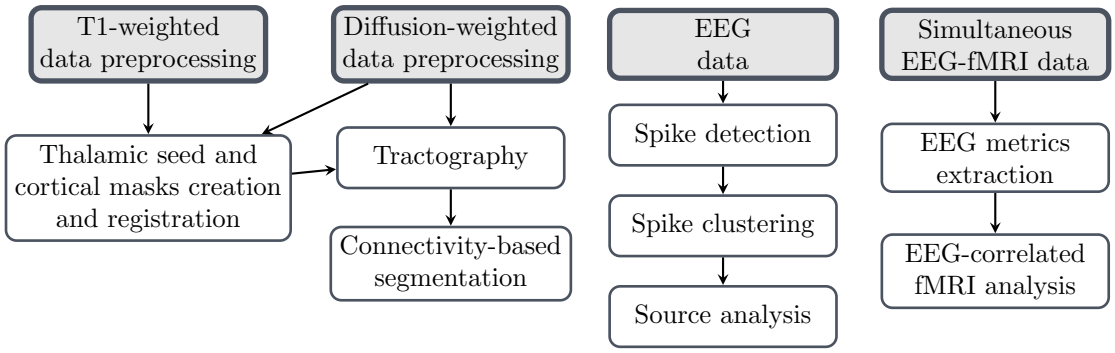


Figure 1: Schematic diagram of the processing pipeline. Firstly, image data had to be preprocessed. Thalamic seed and cortical masks needed to be created and transformed into the diffusion space. Finally, DWI scans were submitted to tractography and the thalamus was parcellated in a hard segmentation way. Whole-night EEG recordings underwent spike detection, followed by spike clustering and finally, source analysis. Regarding the functional images, two EEG regressors of interest were extracted from simultaneously recorded EEG signal in order to perform an EEG-correlated fMRI analysis, to identify the network of brain regions correlated with the occurrence of epileptic activity as measured by the EEG.

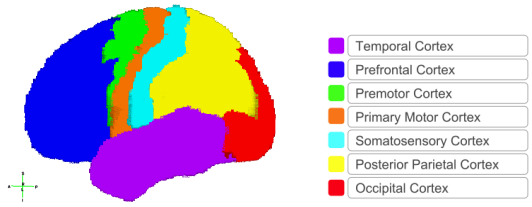


(a) (b)

Figure 2: (a) 3D lateral view of the cerebral cortex considering the 7 divisions according to Brainnetome atlas in the MNI space. The color scheme is as in (b).

ters were coarsely inspected to identify single paroxysmal events that might be corrupting the results; the remaining clusters were subjected to a more detailed analysis, in order to evaluate the consistency of its spikes and the signal to noise ratio, that is, if a spike was easily distinguishable from the background. Spikes within each cluster that survived the previous criterion were averaged, yielding a time course of 1 second each.

*Source analysis.* Localization of the spike activity of CSWS was performed using a realistic boundary element model (BEM), obtained from segmentation of the anatomical T1 image for each patient. Source analysis was computed with the standard low-resolution tomography (sLORETA) method in the cortex found with the BEM. For all individuals, scalp maps of each cluster, along with the source analysis were recorded at half-peak - or, if present, at the peak of the short spike that preceded the main one - and peak amplitude of the global field power (GFP). This was done using the CURRY 6.0 software (Compumedics-Neuroscan).

### 2.4. fMRI data analysis

The fMRI data used here - only available for patient 2 - had already been preprocessed for motion correction and slice timing (Abreu et al., 2018) and therefore no more corrections were applied.

*EEG metrics extraction.* Phase Synchronization Index (PSI) predictor was calculated between two pairs of electrodes, the first yield the highest amplitude on the average interictal epileptiform discharges (IED) - which in this case corresponds to Fp2 - and the other is the one which, together with the first channel exhibited the highest temporal variance - FC6 for this dataset. Unitary Regressor (UR) consists of visually inspect the epileptiform discharges and then model them as stick functions.

*EEG-correlated fMRI analysis.* The rsfMRI data analysis was performed using a general linear model (GLM) framework. Two GLMs were built, after extracting two EEG regressors of interest from simultaneously recorded EEG signal - the UR and PSI. Each regressor had already been computed and convolved with a canonical, double-gamma hemodynamic response function (HRF) for the purpose of Abreu et al. (2018) study. Both the HRF-convolved regressor and the respective time derivative - to account for some degree of intra-subject HRF variability - were included in the model. Statistical significance levels were cluster-corrected, procedure based on Random Gaussian Field theory for correction of multiple comparisons, with voxel $Z > 2.3$ and cluster $p < 0.05$. This was conducted using the FEAT tool (Woolrich et al., 2001).

*Correlation with DWI analysis.* In order to understand in which brain regions the network activation is more prone to occur, for each target ROI, the number of voxels significantly active within each region was computed. To ad-

just for the volume of the target ROIs, those values where divided by the target's number of voxels. The ROIs used here consist of a finer division of the 7-fold cortex parcellation previously made, with 13 distinct and non-overlapping areas: Temporal Superior (TS), Temporal Inferior-lateral (TIL), Temporal Medial (TM), Prefrontal Medial (PFM), Prefrontal Orbitofrontal (PFO), Prefrontal Dorsolateral (PFD), Premotor (PMC), Primary Motor (M1), primary and secondary Somatosensory (S12), Posterior Parietal Medial (PPM), Posterior Parietal Lateral (PPL), Occipital Medio-ventral (OM) and Occipital Lateral (OL).

## 3. Results

### 3.1. Thalamus parcellation

Final thalamic parcellation is depicted in Fig. 3 and the quantification of each thalamic nucleus is presented in Fig. 4. A nuclei organization similar to Behrens et al. (2003a) can be identified.

Given that all subjects present a functional integrity of the sensory and visual thalamocortical relays and absence of afferent somatic-sensory or visual deficits (Leal et al., 2018), somatosensory, premotor and primary motor thalamic nuclei are not considered so relevant for this analysis as the remaining areas. As a consequence, these groups were added in order to be represented together. This procedure also had the advantage of waning the differences in size between the different targets, therefore avoiding that small differences in small thalamic nuclei could yield substantial percentage differences.

In the light of bigger differences between hemispheres corresponding to larger disconnections, one can interpret Fig. 4 as follows: subject 1 presents more disconnection to the prefrontal, temporal and occipital lobes; subject 2 to the temporal and posterior parietal; subject 3 has larger disconnections to the temporal and occipital regions and subject 4's temporal and posterior parietal regions are the most disconnected from the thalamus.

Fig. 5 depicts the same results as figure Fig. 4, however, in this case, imposing a 50% threshold of probability of connection to cortex, *prior* to the hard segmentation.

When this threshold is applied, only probabilities of connection to each target mask above 50% are considered. This step improves the confidence on the clusters obtained. Considering that in this case the nuclei appear smaller, small differences between hemispheres could yield bigger percentual differences, nonetheless, this difference, with this threshold, is likely to be more reliable. These results are in agreement with the previous ones: the temporal nucleus is still the most affected in all patients and the posterior parietal nucleus seems to be more disconnected than before, in particular for subject 3, almost to equal extents as the previously found for the occipital nucleus. The preponderance of the occipital nucleus, in this analysis, is more evident in subject 4 - even more than the posterioparietal region previously found - and less evident in subject 1, where frontal and temporal regions seem to be the most affected.

### 3.2. EEG results

A summary of the source analysis for each patient and each cluster can be found in Fig. 6.

A spike concentration in the temporal lobe was found for patient 1, both at the half peak and peak amplitudes. A localization near the borders of the temporal with the posterior parietal cortex was detected for half of the clusters analyzed at the peak. All spikes were present in the hemisphere of the thalamic lesion, the right one.

A more distributed pattern of clusters was found for subject 2. One cluster showed signs of propagation, that is, the intracranial generator did not remain in the same position (or orientation) during the entire epileptiform discharge. In this case, it suffered a shift from the posterior parietal to the prefrontal cortex. Another one seemed to be initiated at the prefrontal cortex with propagation to the central region of the brain and other single case suggested a propagation from the occipital region to the temporal cortex. The other 4 remained at the occipital region during the paroxysmal event. The spike sources for this patient were not restricted to the lesioned hemisphere (right), indeed some of them were localized in the healthy left hemisphere, but, always adjacent to the medial plane. At the peak, there were 3 spikes in this situation and at half peak only one. It is also worth pointing out, that the topographic maps suggested a frontal *foci*, in clusters 1 to 5. However this was not depicted in the source maps obtained, which can be due to a mislocation due to the small number of electrodes used for the source analysis.

As for subject 3, a propagation of the epileptic activity from the posterior to the anterior region was clear. From the 16 clusters analyzed, 14 moved from the occipital to the prefrontal cortex, whereas the other two remained in the frontal cortex during the entire IED. In all cases, spikes were localized in the left (lesioned) hemisphere. Occiptal spikes, despite being located in the occipital lobe, showed a position which is near the borders between the occipital and temporal lobes and the posterior parietal lobes.

Subject 4 had a substantial concentration of spikes in the occipital cortex at half peak. Only one cluster was localized in the prefrontal cortex at this time point and during the peak it suffered a shift to a more posterior region, near the central brain. The remaining 13 clusters continued to appear in occip-

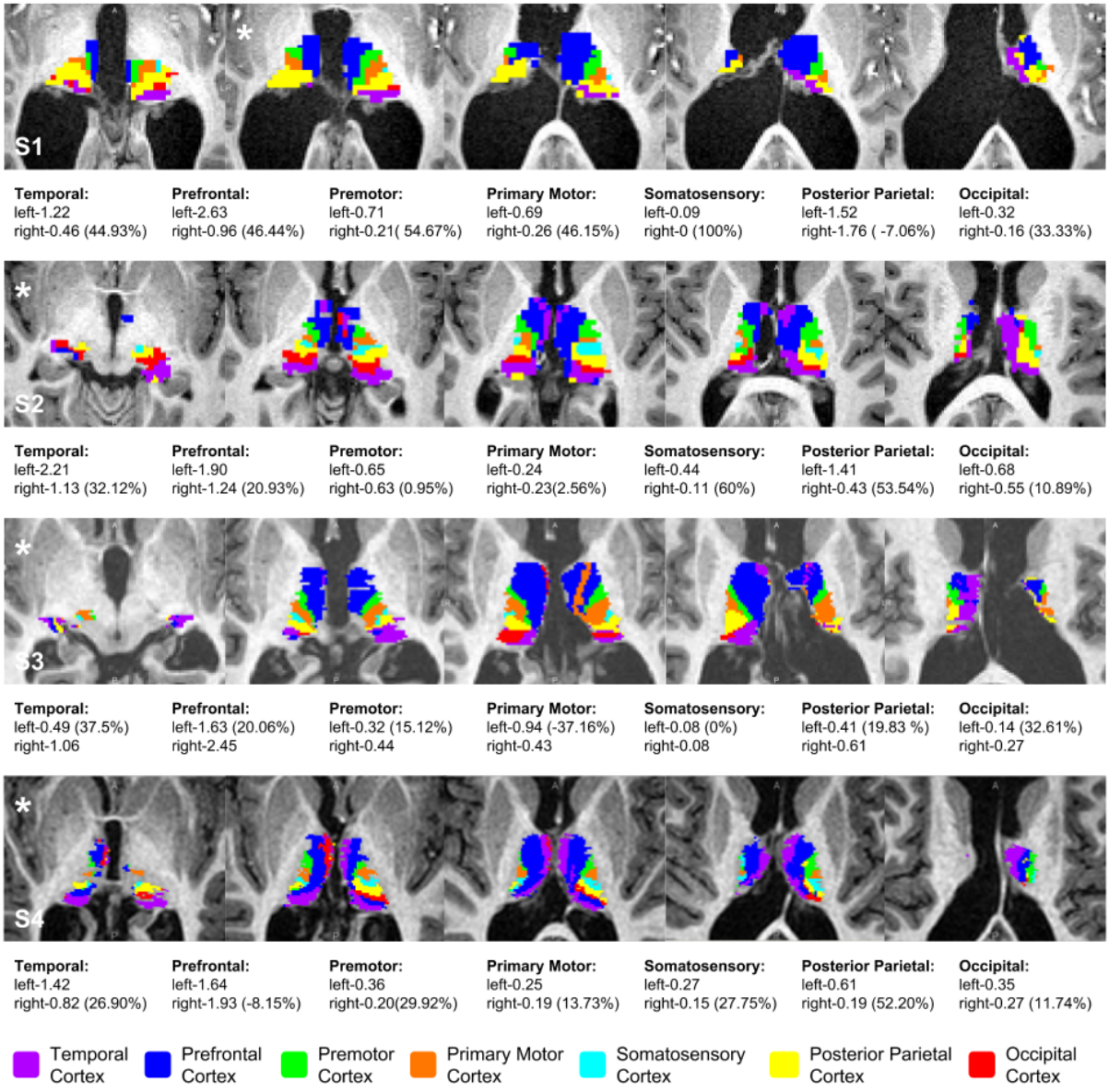


Figure 3: 7-fold thalamic parcellation for each subject. Slices are shown 4 mm apart from each other, along the vertical axis of the reference system. Below each set of images there is the corresponding volumetric results (in m$L$) of each group identified in the thalamic parcellation. In brackets is shown the relative volume of the nucleus in the hemisphere ipsilateral to the thalamic lesion compared with the unaffected one in the healthy contralateral hemisphere. * symbol identifies the AC-PC plane in each subject. Note that subject 3 has a lesion in the left hemisphere, as opposed to the remaining subjects where a right lesion is present.

tal positions, nevertheless a slight shift towards the the anterior direction seemed to be visible. Indeed, 5 out of those 13, at the peak, assumed a position at the border between the temporal and occipital regions. Spike *foci* for subject 4 were confined to the hemisphere of the thalamic lesion (right).

### 3.3. fMRI results

Results for the use of UR and PSI metrics as predictors to the epilepsy-related rsfMRI fluctuations are shown in figure Fig. 7.

Results are consistent with Abreu et al. (2018) work. Equally to their results, the epileptic networks obtained using the UR or the PSI predictors yielded slightly different results. Overall, the networks of brain regions correlated with the occurrence of epileptic activity were in agreement with results from the whole-night EEG recordings for this patient (Fig. 6). Indeed, these showed evidence of epileptic activity propagation from the posterior to

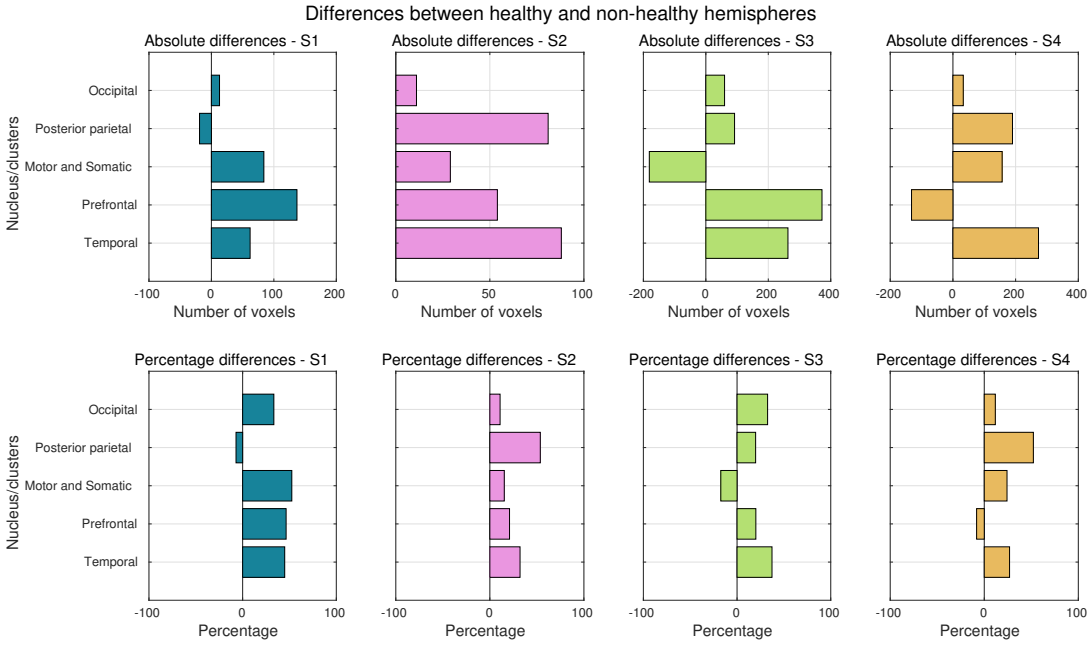


Figure 4: Volume differences between the healthy and non-healthy hemispheres. Absolute values - top row and percentage values - bottom row. Absolute values are expressed in number of voxels. Notice that absolute numbers are calculated in the space of each subject, whereby comparison between subjects is not adequate as it does not take into account differences in total brain volumes.

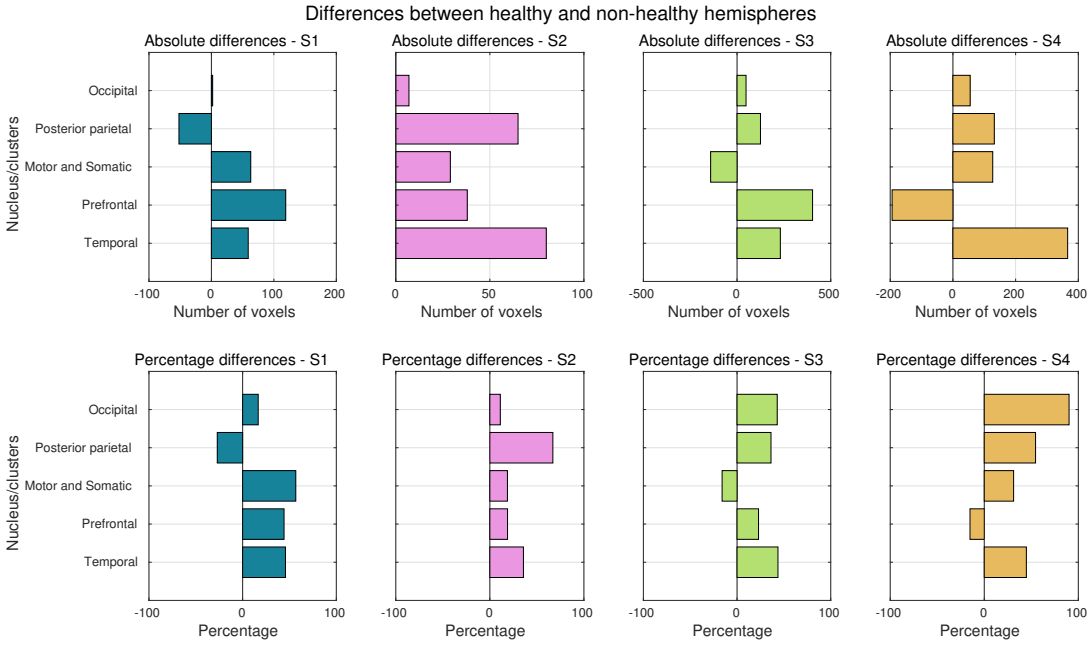


Figure 5: Volume differences between the healthy and non-healthy hemispheres for thalamic clusters thresholded at 50% probability of connection to cortex. Absolute values - top row and percentage values - bottom row. Absolute values are expressed in number of voxels. Notice that absolute numbers are calculated in the space of each subject, whereby comparison between subjects is not adequate as it does not take into account differences in total brain volumes.

the anterior lobes and a bilateral involvement of the occipital cortex.

## 4. Discussion

### 4.1. Thalamic lesions overview

It is important to notice that, while, in general, the healthy hemisphere contains bigger nuclei than the lesioned hemisphere - a result which is not sur-

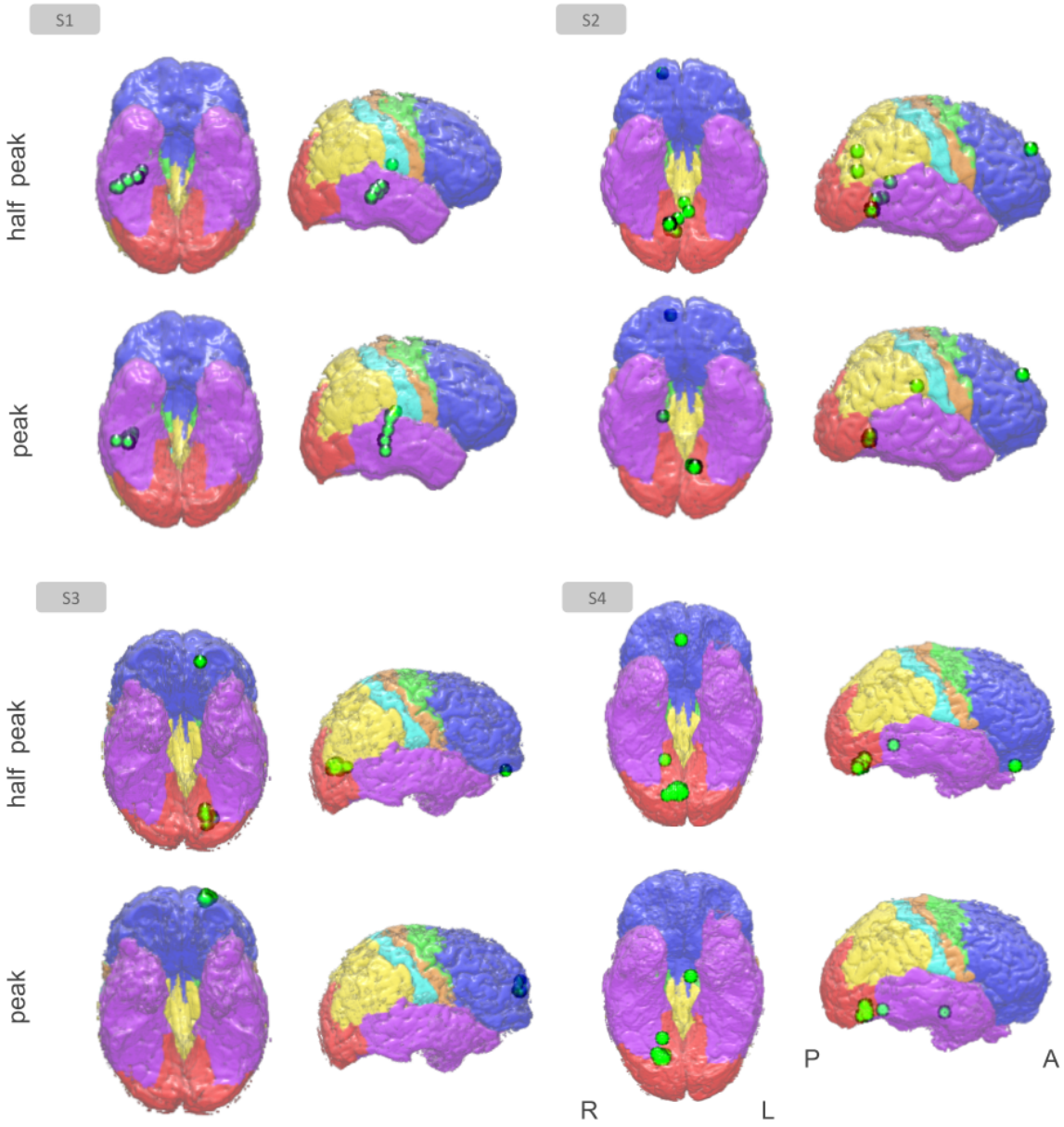


Figure 6: 3D inferior and right views of the 7-fold cortical parcellation for each patient. Color scheme in agreement with the one in figure 2. For each subject and for two distinct time points - half peak and peak amplitudes of the GFP - it is displayed in green the dipoles obtained from the source analysis with sLORETA. Each dipole corresponds to one cluster of IEDs. There are some dipoles which overlap spatially. Images obtained with software MRICroGL (University of South Carolina).

prising given that the the thalamus of the latter hemisphere suffered a wide spread volume loss, from 19% to a massive 94%, as calculated by Leal et al. (2018), for these patients - there were some nuclei where the opposite occurred, namely, the posterior parietal, the motor and somatic and the prefrontal thalamic nuclei in subjects 1, 3 and 4, respectively. This might be explained by the loss of corticothalamic or thalamocortical fibers in adjacent regions of a given nucleus, in the non-healthy hemisphere, which may have resulted in a decrease in competition when applying the "winner takes-it-all" algorithm. This can lead to the classification of the neighbouring voxels of those nuclei as also belonging to the nucleus itself. As a consequence, they appear bigger in volume, with respect to those in the contralateral hemisphere.

Thalamocortical connections with the temporal cortex were mainly affected in all the study patients, followed by the posterior parietal cortex and occipital cortex in half of the patients. Prefrontal cortex connections with the thalamus seemed to be

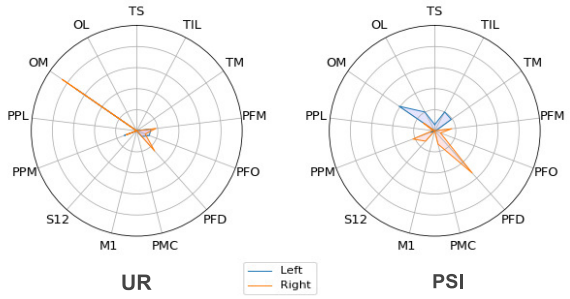


Figure 7: Radar plots using UR (left) and the PSI (right). The values indicate the relative number of voxels significantly activated in left (blue) and right (orange) hemispheres in each of the cortical targets. Targets correspond to the 13-fold cortical parcellation presented in Implementation.

affected only in patient 1. This is the subject with the most severe CSWS, also the one presenting the greatest enlargement of the ventricles. Inspecting Fig. 4 closely, one realizes that 3 of the 4 main brain lobes (parietal, frontal and temporal) present an almost 50% reduction in the volume of its respective thalamic nuclei in the lesioned hemisphere.

On the whole, the results obtained here show diminished thalamic nuclei volumes on the lesioned hemisphere. In addition, nuclei with main connections to the temporal, posterior parietal and occipital cortical regions seemed to be mostly affected in the majority of the subjects. This observation correlates well with the fact that in all cases the thalamic lesion affects mostly the mediodorsal and pulvinar nuclei. Indeed, it is the pulvinar which typically presents the most connections with the temporal and posterior parietal cortex. Mediodorsal nuclei project mainly to the prefrontal cortex, and despite being affected, seems to be to a lesser extension when compared to the pulvinar.

### 4.2. Cortical origin of spikes

Our results suggest the involvement of the posterior brain quadrant before the occurrence of the spike peak. At the spike peak amplitude, however, evidence points towards the involvement of both the anterior and posterior quadrants. This change in electrical scalp configuration suggests a shift of the intracranial generators from the posterior brain areas early in the spike to more anterior brain generators later on, at spike peak.

Its is worth pointing out the method used to map the paroxysmal events. Given that the paroxysmal activity, in these patients, is multifocal, it is naive to derive the epileptic activity distribution from just one spike, even if one finds it representative of all spikes present in a typical EEG recording. This *a priori* choice of a given paroxistic event, may lead to serious problems of representativeness. On the contrary, if all the spikes are taken into account in a non biased method to derive a spatial representation of the epileptic activity, a more accurate and more realistic image should be obtained and its relationship with corticothalamic disconnection evaluated.

Regarding the epileptic networks obtained for subject 2 using the UR or the PSI predictors, it can be noted that while the UR demonstrates clearly activated regions both in the frontal and occipital medial cortex, the PSI predictor shows activation essentially in the occipital area, more predominantly on the left side. This might be explained by IEDs of considerably higher amplitude being located in the frontal region, despite the hypothesized epileptic focus being located in posterior regions (Abreu et al., 2018). Fig. 6 also illustrates the presence of a cluster in the frontal cortex and the remaining 6 on the posterior lobes. Regarding the presence of extensive activation in the left side, even though the lesion is in the right thalamus, these authors also presented a source analysis for this patient, using a different algorithm from the one used here, where an occipital right region is identified as being in the origin of this epileptic activity, despite the left activation.

### 4.3. Model of origin of CSWS

Leal et al. (2018) postulated that the corticothalamic brain disconnection in the patients with unilateral thalamic lesions might express a frequency-dependent increased excitability around the 10 Hz of sleep-spindles. This is supported by the preserved sleep spindles in the hemisphere of the thalamic lesion in these patients (Leal et al. (2018)). Also, as observed by these authors, when subjected to corticocortical stimulation of 10-20 Hz, these patients demonstrated a frequency-dependent increased excitability. Previous literature also supports this hypothesis: Battaglia et al. (2009) observed the disappearance of CSWS after an hemispherectomy - surgical procedure which disconnects the cortex from the thalamus, and so, from sleep spindles. Furthermore, these patients show no frequency-dependent excitability at spindle frequency, after CSWS resolution (Leal et al., 2018).

The variation of sleep-spindles through the wake-sleep cycle is explained by the low cholinergic tonus present in stages of non-REM sleep. (Fernández et al., 2012a) The augmenting response has also been shown to be dependent on the cholinergic tonus of the cortex, which typically is high in wakefullness and REM sleep, and low in non-REM sleep (Timofeev and Steriade, 1998). Because augmenting responses typically is increased at low cholinergic tone, this could be an additional factor explaining the increased susceptibility of non-REM sleep

to this pathological synaptic plasticity. The disappearance of CSWS with wakefulness and REM sleep, was again verified in this case by Leal et al. (2018).

The combination of the previous observations, lead these authors to propose a model for the genesis of CSWS in patients with unilateral thalamic lesions that consisted on having a cortical area partially deafferented from the dorsal thalamus, sparing the ventral thalamus (which includes the reticular nucleus, one of the structures of the sleep-spindles generator). This disconnection between the thalamus and the cortex would express a pathologically increased augmenting response at the frequencies of the sleep-spindles. This growing cortical potential, which underlies a more robust and highly synchronized neural activity, in turn, leads to the spike-wave paroxysmal events.

## 5. Conclusions

The etiology of CSWS is currently unknown but the thalamus has been demonstrated to play a key role in its genesis. The objective of this thesis was to parcellate the thalamus of 4 individuals with unilateral thalamic lesions, into its nuclei. This parcellation was used to infer about the structural connectivity between each thalamic nuclei and different cortical regions of the brain.

The results obtained in this thesis seem to corroborate the hypothesis proposed by Leal et al. (2018) for the genesis of CSWS in patients with unilateral thalamic lesions. Firstly, in general, for all patients, results from tractographic parcellation identified the posterior regions as the brain areas with most thalamic disconnectivity. Secondly, EEG results found a posterior brain pattern for the paroxysmal activity of these children.

Taking both these points into consideration, the overall pattern of thalamocortical disconnectivity found in this thesis is fairly in line with the distribution of epileptic activity observed, consistent with a posterior brain region more disconnected from the thalamus, as well as more prone to paroxysmal activity. These results provide further support to the hypothesis of a causal role of a cortex partially disconnected from thalamic inputs being responsible for the genesis of epileptic activity, in patients with this pattern of thalamic lesions. Patient 1, however, has clear signs of disconnectivity from the prefrontal cortex; nevertheless, epileptic activity is not apparent in the anterior quadrant, which suggests that other factors may exist promoting epileptic *foci* in the posterior, rather than the anterior brain.

Despite the results obtained, more work should be done in this field to validate this hypothesis. Testing this model in other etiologies, such as the Landau-Klefener syndrome would be of interest. Children with this syndrome, similar to CSWS, possess verbal agnosia; this is, an inability to understand spoken language that can mimic deafness (Fernández et al., 2012a). A thalamocortical disconnection limited to the spatial extent of the language processing areas would help to validate the applicability of this model and the used parcellation methodology.

In addition, WM atrophy quantification for each brain region, which was not conducted in this thesis, could be implemented. This course of action would be essential to prove the concept of a neocortical area partially deafferented from the thalamus and would be complementary to the analysis already performed using the diffusion principle.

Since the subjects under analysis are children, it would be recommend that the delimitation of the cortical areas would be done manually in an infant template, as the one provided by McConnell Brain Imaging Centre. Finally, future prospective works should address and overcome the fact that not all patients underwent the same investigation and that the data was not acquired in an equal manner for every patient, due to the retrospective exploratory character of the present study and to patient cooperation constraints.

## Acknowledgements

I would like to express my appreciation to professor Rita Nunes, professor Patrícia Figueiredo and Dr. Alberto Leal for their guidance through this work; and to my family and friends for their exceptional support.

## References

Abreu, R., Leal, A., da Silva, F. L., and Figueiredo, P. Eeg synchronization measures predict epilepsy-related bold-fmri fluctuations better than commonly used univariate metrics. *Clinical Neurophysiology*, 129(3):618–635, 2018.

Andersson, J. L. and Sotiropoulos, S. N. An integrated approach to correction for off-resonance effects and subject movement in diffusion mr imaging. *Neuroimage*, 125: 1063–1078, 2016.

Avants, B. B., Tustison, N. J., Song, G., Cook, P. A., Klein, A., and Gee, J. C. A reproducible evaluation of ants similarity metric performance in brain image registration. *Neuroimage*, 54(3):2033–2044, 2011.

Bastiani, M. and Roebroeck, A. Unraveling the multi-scale structural organization and connectivity of the human brain: the role of diffusion mri. *Frontiers in neuroanatomy*, 9:77, 2015.

Battaglia, D., Veggiotti, P., Lettori, D., Tamburrini, G., Tartaglione, T., Graziano, A., Veredice, C., Sacco, A., Chieffo, D., Pecoraro, A., et al. Functional hemispherectomy in children with epilepsy and csws due to unilateral early brain injury including thalamus: sudden recovery of csws. *Epilepsy research*, 87(2-3):290–298, 2009.

Behrens, T. E., Johansen-Berg, H., Woolrich, M., Smith, S., Wheeler-Kingshott, C., Boulby, P., Barker, G., Sillery, E., Sheehan, K., Ciccarelli, O., et al. Non-invasive mapping

of connections between human thalamus and cortex using diffusion imaging. *Nature neuroscience*, 6(7):750, 2003a.

Behrens, T. E., Woolrich, M. W., Jenkinson, M., Johansen-Berg, H., Nunes, R. G., Clare, S., Matthews, P. M., Brady, J. M., and Smith, S. M. Characterization and propagation of uncertainty in diffusion-weighted mr imaging. *Magnetic Resonance in Medicine: An Official Journal of the International Society for Magnetic Resonance in Medicine*, 50 (5):1077–1088, 2003b.

Behrens, T. E., Berg, H. J., Jbabdi, S., Rushworth, M. F., and Woolrich, M. W. Probabilistic diffusion tractography with multiple fibre orientations: What can we gain? *Neuroimage*, 34(1):144–155, 2007.

Cloutman, L. L., Ralph, L., and Matthew, A. Connectivity-based structural and functional parcellation of the human cortex using diffusion imaging and tractography. *Frontiers in neuroanatomy*, 6:34, 2012.

Fan, L., Li, H., Zhuo, J., Zhang, Y., Wang, J., Chen, L., Yang, Z., Chu, C., Xie, S., Laird, A. R., et al. The human brainnetome atlas: a new brain atlas based on connectional architecture. *Cerebral cortex*, 26(8):3508–3526, 2016.

Fernández, I. S., Loddenkemper, T., Peters, J. M., and Kothare, S. V. Electrical status epilepticus in sleep: clinical presentation and pathophysiology. *Pediatric neurology*, 47(6):390–410, 2012a.

Fernández, I. S., Takeoka, M., Tas, E., Peters, J., Prabhu, S., Stannard, K., Gregas, M., Eksioglu, Y., Rotenberg, A., Riviello, J., et al. Early thalamic lesions in patients with sleep-potentiated epileptiform activity. *Neurology*, 78(22): 1721–1727, 2012b.

Guzzetta, F., Battaglia, D., Veredice, C., Donvito, V., Pane, M., Lettori, D., Chiricozzi, F., Chieffo, D., Tartaglione, T., and Dravet, C. Early thalamic injury associated with epilepsy and continuous spike–wave during slow sleep. *Epilepsia*, 46(6):889–900, 2005.

Incorpora, G., Pavone, P., Smilari, P., Trifiletti, R., and Parano, E. Late primary unilateral thalamic hemorrhage in infancy: report of two cases. *Neuropediatrics*, 30(05): 264–267, 1999.

Jenkinson, M. and Smith, S. A global optimisation method for robust affine registration of brain images. *Medical image analysis*, 5(2):143–156, 2001.

Kelemen, A., Barsi, P., Gyorsok, Z., Sarac, J., Szűcs, A., and Halász, P. Thalamic lesion and epilepsy with generalized seizures, eses and spike-wave paroxysmsreport of three cases. *Seizure*, 15(6):454–458, 2006.

Kersbergen, K. J., de Vries, L. S., Leijten, F. S., Braun, K. P., Nievelstein, R. A., Groenendaal, F., Benders, M. J., and Jansen, F. E. Neonatal thalamic hemorrhage is strongly associated with electrical status epilepticus in slow wave sleep. *Epilepsia*, 54(4):733–740, 2013.

Klein, A., Andersson, J., Ardekani, B. A., Ashburner, J., Avants, B., Chiang, M.-C., Christensen, G. E., Collins, D. L., Gee, J., Hellier, P., et al. Evaluation of 14 nonlinear deformation algorithms applied to human brain mri registration. *Neuroimage*, 46(3):786–802, 2009.

Leal, A., Calado, E., Vieira, J. P., Mendonça, C., Ferreira, J. C., Ferreira, H., Carvalho, D., Furtado, F., Gomes, R., and Monteiro, J. P. Anatomical and physiological basis of continuous spike–wave of sleep syndrome after early thalamic lesions. *Epilepsy & Behavior*, 78:243–255, 2018.

Losito, E., Battaglia, D., Chieffo, D., Raponi, M., Ranalli, D., Contaldo, I., Giansanti, C., De Clemente, V., Quintiliani, M., Antichi, E., et al. Sleep-potentiated epileptiform activity in early thalamic injuries: study in a large series (60 cases). *Epilepsy research*, 109:90–99, 2015.

Monteiro, J. P., Roulet-Perez, E., Davidoff, V., and Deonna, T. Primary neonatal thalamic haemorrhage and epilepsy with continuous spike-wave during sleep: a longitudinal follow-up of a possible significant relation. *European Journal of Paediatric Neurology*, 5(1):41–47, 2001.

Power, B. D., Wilkes, F. A., Hunter-Dickson, M., van Westen, D., Santillo, A. F., Walterfang, M., Nilsson, C., Velakoulis, D., and Looi, J. C. Validation of a protocol for manual segmentation of the thalamus on magnetic resonance imaging scans. *Psychiatry Research: Neuroimaging*, 232(1):98–105, 2015.

Scheuer, M. L., Bagic, A., and Wilson, S. B. Spike detection: Inter-reader agreement and a statistical turing test on a large data set. *Clinical Neurophysiology*, 128(1):243–250, 2017.

Sherman, S. M. and Guillery, R. W. *Functional connections of cortical areas - a new view from the thalamus*. MIT Press, 2013.

Singhal, N. S. and Sullivan, J. E. Continuous spike-wave during slow wave sleep and related conditions. *ISRN neurology*, 2014, 2014.

Smith, S. M. Fast robust automated brain extraction. *Human brain mapping*, 17(3):143–155, 2002.

Steriade, M. and Timofeev, I. Short-term plasticity during intrathalamic augmenting responses in decorticated cats. *Journal of Neuroscience*, 17(10):3778–3795, 1997.

Timofeev, I. and Steriade, M. Cellular mechanisms underlying intrathalamic augmenting responses of reticular and relay neurons. *Journal of Neurophysiology*, 79(5):2716–2729, 1998.

Timofeev, I., Grenier, F., Bazhenov, M., Houweling, A. R., Sejnowski, T. J., and Steriade, M. Short-and medium-term plasticity associated with augmenting responses in cortical slabs and spindles in intact cortex of cats in vivo. *The Journal of physiology*, 542(2):583–598, 2002.

Woolrich, M. W., Ripley, B. D., Brady, M., and Smith, S. M. Temporal autocorrelation in univariate linear modeling of fmri data. *Neuroimage*, 14(6):1370–1386, 2001.

Zhang, Y., Brady, M., and Smith, S. Segmentation of brain mr images through a hidden markov random field model and the expectation-maximization algorithm. *IEEE transactions on medical imaging*, 20(1):45–57, 2001.